FINITE ELEMENT ANALYSIS OF REINFORCED MASONRY SHEAR WALLS USING SMEARED CRACK MODEL

Majid Maleki[1], A. A. El-Damatty[2], A. A. Hamid[3] and R. G. Drysdale[4]

[1]Ph.D. Candidate, Department of Civil Engineering, McMaster University, 1280 Main St. WEST, Hamilton, ON, L8S 4L7, malekim@mcmaster.ca

[2]Associate Professor, Department of Civil and Environmental Engineering, The University of Western Ontario, damatty@uwo.ca

[3]Adjunct Professor, Department of Civil Engineering, McMaster University, hamida@mcmaster.ca

[4]Professor, Department of Civil Engineering, McMaster University, drysdale@mcmaster.ca

ABSTRACT

This paper provides an evaluation of the capability of a layered finite element model using smeared crack approach to capture the behaviour of fully grouted fully reinforced masonry shear walls subject to in-plane loading. Tension stiffening, compression softening, as well as strength degradation of the grouted concrete block parallel to the crack direction are included in this model. The comparison between analytical and experimental results showed good agreement in prediction of pre- and post-peak response for different failure modes, although in shear dominated failure some differences were observed.

KEYWORDS: finite element, smeared crack, reinforced masonry, tension stiffening, orthotropic

INTRODUCTION

Significant heterogeneity and anisotropy of masonry structures resulting from the presence of clay or concrete units, mortar, grout, and steel bars have created one of the most challenging composites for numerical simulation. In addition to the variety of the constituent component, the highly nonlinear and asymmetric stress-strain relationship of the materials and great complexity of the interaction between them have increased the number of difficulties in developing an accurate modelling method that can adequately predict the behaviour and different modes of failure of this system of construction. Nevertheless, to date, diverse types of numerical techniques have been developed to enhance the basic understanding of the pre- and post-peak responses of masonry components with particular emphasis on shear walls as the main lateral loadbearing elements in "box" type buildings.

A finite element model that accounts for the nonlinear behaviour of masonry was developed and applied to solid masonry by Page [1] in 1978 from the analogy of the behaviour of masonry assemblages and jointed rocks. Subsequently, many researchers have developed various homogenized [2] and heterogenized [1, 3, 4] modeling methods to capture the in-plane and out-of-plane response of masonry shear walls.

A recent technique for modeling reinforced concrete and masonry uses a layered finite element based on smeared crack model in which idealized layers of concrete and steel represent the actual behaviour of the corresponding constituent material and the cracking effect is assumed to be smeared over the entire hybrid element [3, 5]. This paper contains an evaluation of using this technique in predicting behaviour of fully grouted reinforced masonry shear walls. Tension stiffening, compression softening as well as strength degradation parallel to the crack direction are included in this model. Since other studies show that the solid grout and concrete masonry units form the bulk of the masonry, the anisotropy and plane of weakness introduced by mortar joints are neglected [3].

ANALYTICAL MODEL

The proposed smeared crack approach is known as the rotating crack model in which the principal axes of stress and strain are continuously updated prior to and after cracking. Experimental evidence [6] has shown that, due to aggregate interlock forces along the crack surface and dowelling action of reinforcement bars, using a fixed crack model can be misleading especially for walls subjected to dynamic or cyclic loadings. The adopted smeared crack model and the constitutive relations of the materials are described in the following sections.

STRENGTH FAILURE ENVELOPE

In shear dominated components like panels and shear walls, various combinations of biaxial principal stress (σ_1, σ_2) exist due to combined axial and lateral load resulting in different behaviour compared to uniaxial loading. A *Compression-compression* biaxial state of stress offers microcrack confinement and increases the uniaxial compressive strength of masonry, f'_m, according to the following model proposed by Kupfer et. al. [7] and also used in TCCMAR research program [5]:

$$\lambda = \frac{\left(1+\sigma_1/\sigma_2\right)^2}{1+A_0\sigma_1/\sigma_2} \qquad 0 \le \sigma_1/\sigma_2 \le 1 \qquad \text{Equation 1}$$

$$\varepsilon_p = \varepsilon_o/\lambda \qquad \text{Equation 2}$$

$$f_p = f'_m/\lambda \qquad \text{Equation 3}$$

where ε_o is the uniaxial strain corresponding to uniaxial compressive strength f'_m, ε_p and f_p are the peak compressive strain and stress of the masonry after biaxial stress enhancement, and λ is the strength modification factor. The parameter A_0 is used to calibrate the model based on the material properties. The suggested value [7] is $A_0 = 3.65$ for concrete. Although it is employed here, further studies need to be conducted for masonry applications.

On the other hand, a *tension-compression* stress state can significantly reduce the peak strength of masonry in compression. Tests on reinforced concrete panels [8] show that this reduction is a function of lateral tensile strain, ε_1, rather than equivalent tensile stress, σ_1, at the instant of cracking. The following equation [8] employs β as a reduction factor to define this behaviour. It is also assumed that the elastic behaviour in tension is not affected by lateral compressive stress.

$$\beta = \frac{1}{0.8 - 0.34\varepsilon_1 / \varepsilon_o} \le 1.0 \qquad \text{Equation 4}$$

$$\varepsilon_p = \beta \varepsilon_o \qquad \text{Equation 5}$$

$$f_p = \beta f'_m \qquad \text{Equation 6}$$

In the *tension-tension* biaxial combination of stresses, the tensile strength remains equal to the uniaxial tensile strength in both directions of principal strains.

STRESS-STRAIN RELATIONS IN PRINCIPAL DIRECTIONS

In compression, the stress-strain relation shown in Figure 1, is similar to others widely used in concrete and masonry research [3, 9, 10]. The initial parabolic relation is followed by a strain softening branch which smoothly links to an exponential tail at very high strains. The equations adopted from TCCMAR research program [5] for behaviour of masonry in compression are:

$$\sigma(\varepsilon) = f'_m \left[A_1 (\varepsilon/\varepsilon_o) - \lambda (A_1 - 1)(\varepsilon/\varepsilon_o)^2 \right] \qquad 0 \ge \varepsilon \ge \varepsilon_p \qquad \text{Equation 7}$$

$$\sigma(\varepsilon) = f_p \left[1 - \frac{(\varepsilon - \varepsilon_p)^2}{(A_2 \varepsilon_o - \varepsilon_p)^2} \right] \qquad \varepsilon_p > \varepsilon \ge \varepsilon_e \qquad \text{Equation 8}$$

$$\sigma(\varepsilon) = f_e \left[A_3 (f_m / f_e) + \left(1 - A_3 (f_m / f_e) \exp\left[-\gamma \frac{(\varepsilon - \varepsilon_e)}{\varepsilon_e} \right] \right) \right] \qquad \varepsilon < \varepsilon_e \qquad \text{Equation 9}$$

where A_1 controls the shape of the rising branch and its value can range from 1.0 to 2.0 (A_1=1 defines a straight line from the origin to the peak strength and A_1=2.0 gives a parabolic shape to the curve). A_2 controls the shape of the initial falling branch and its value can be greater or equal to 1.0. A_3 alters the lower limit of the exponential falling branch and its value can vary from 0.0 to 1.0. The exponential tail at Equation 9 is attached to Equation 8 at ε_e and f_e is the compressive stress at point of tangency. ε_e is determined by the following equation:

$$\varepsilon_e = \varepsilon_o (1 + A_4 (A_2 - 1)/\lambda) \qquad \text{Equation 10}$$

where A_4 is a shape factor defining the location of the initial point of the exponential tail. The exponential parameter, γ, is determined so that Equation 9 becomes tangent to Equation 8 at ε_e. The parameter γ is defined by:

$$\gamma = \frac{2 f_m}{\lambda f_e} \times \frac{\varepsilon_\varepsilon}{1 - A_3 (f_m / f_e)} \times \frac{(\varepsilon_e - \varepsilon_p)}{(A_2 \varepsilon_o - \varepsilon_p)^2} \qquad \text{Equation 11}$$

According to Equations 2, 3, 5 and 6, the compressive strength and corresponding peak strain increases when the masonry is confined by the biaxial compression stress state and decreases due to lateral tensile stress normal to the principal compressive direction. This implies that, based on

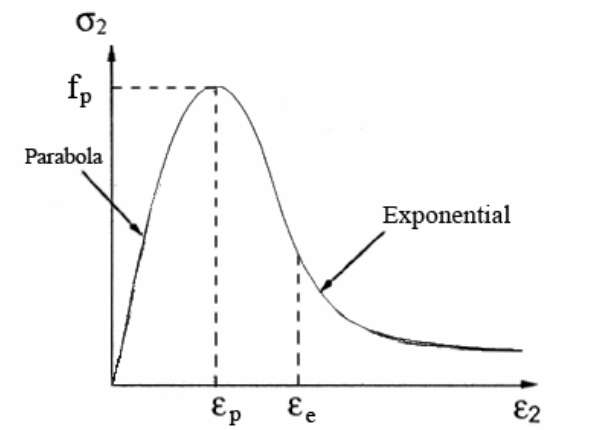

Figure 1 – Stress-strain curve of masonry in compression

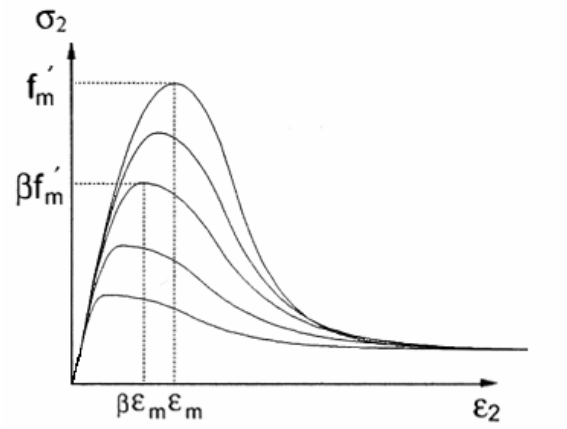

Figure 2 – Strength reduction effect of masonry

the current state of principal stresses and strains, the constitutive relations are continuously updated during the analysis at each step (Figure 2).

In tension, even after a part of the masonry shear wall cracks, the uncracked section retains its capability to resist tensile stress because of the continuity provided by the reinforcing bars. This reserve post-crack strength in tension is known as tension stiffening. Vecchio and Collins [8] described this effect by an exponentially descending branch attached to the cracking point of the stress-strain curve for masonry, (ε_{cr}, f_{cr}), in tension (Figure 3). Consistent with this approach, the stress-strain relation of masonry in tension, including the tension stiffening model in this study, used in TCCMAR research program [5], are defined by:

$$\sigma(\varepsilon) = E_t \varepsilon_t \qquad 0 < \varepsilon_t \le \varepsilon_{cr} \qquad \text{Equation 12}$$

$$\sigma(\varepsilon) = f_{cr}\left[B_1 + (1-B_1)\exp\left[-\alpha\frac{(\varepsilon_t - \varepsilon_{cr})}{\varepsilon_{cr}}\right]\right] \qquad \varepsilon_t > \varepsilon_{cr} \qquad \text{Equation 13}$$

where B_1 controls the lower limit of the exponential branch and α incorporates the effect of steel percentage. The extra stiffness provided by this effect has to reduce to zero once steel reaches its uniaxial yield strain. Table 1 contains suggested values for B_1 and α in reinforced concrete models [5]. Modification may be required for the masonry to obtain an accurate estimate for these parameters.

The failure surface for steel is simply represented by a bilinear strain hardening behaviour which is identical in tension and compression (Figure 4). Since the reinforcing bars are simulated as one-dimensional elements, this model will remain aligned with the bar directions during the analysis. The plastic modulus, E_{sp}, in this model is defined by a bilinear coefficient, ζ, which is independent of level of stress and strain:

$$E_{sp} = \zeta\, E_s \qquad \text{Equation 14}$$

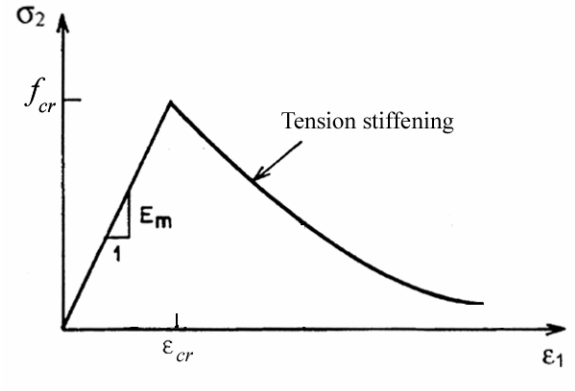

Figure 3 – tension stiffening model

Table 1 - Suggested values for B_1 and α [5]

Percentage of Steel (ρ, %)	α	B_1
0.25	0.06	0.38
0.35	0.10	0.48
0.50	0.18	0.5
0.75	0.25	0.5

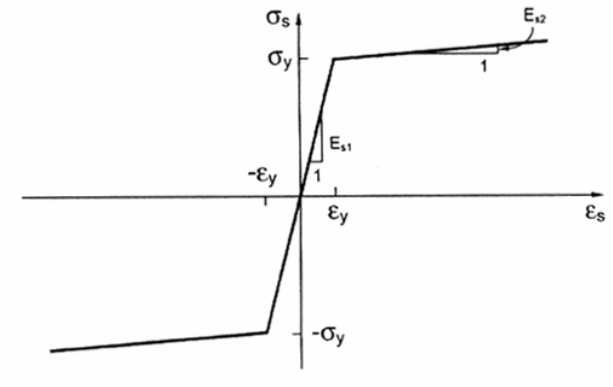

Figure 4 – Stress-strain curve of steel

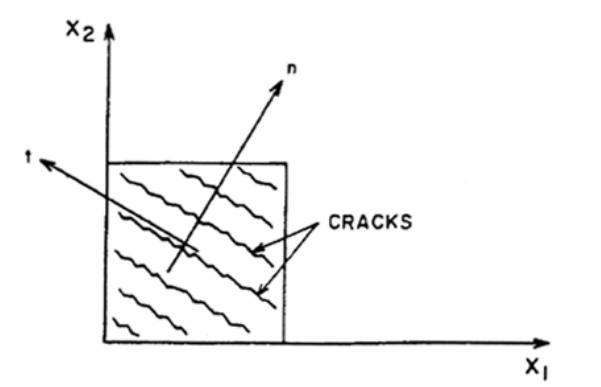

Figure 5 – Smeared crack model

CONSTITUTIVE AND STIFFNESS MATRIX

The constitutive model for masonry is based on orthotropic bimodular behaviour using equivalent uniaxial stress-strain relations along the axes of orthotropy which coincide with the directions parallel and perpendicular to cracks (Figure 5). The constitutive model used for masonry is comprised of two stages. The first stage is applicable prior to tensile cracking and follows the model presented by Darwin and Pecknold [10]:

$$\mathbf{D_m} = \frac{1}{1-\nu^2}\begin{bmatrix} E_1 & \nu(E_1E_2)^{1/2} & 0 \\ \nu(E_1E_2)^{1/2} & E_2 & 0 \\ 0 & 0 & \bar{G} \end{bmatrix} \text{ and } \bar{G} = \frac{E_1 + E_2 - 2\nu(E_1E_2)^{1/2}}{4} \qquad \text{Equation 15}$$

where E_1 and E_2 are the secant moduli of elasticity in the directions of principal axes of strains. ν is the Poisson's ratio and $\bar{G}$ is the secant shear modulus. The off diagonal non-zero terms correspond to the effect of biaxial loading due to lateral tension or compression. However, zero diagonal terms show that interaction between shear and normal strains has been neglected for

simplicity and computational efficiency. After tensile cracking, the constitutive relation is changed to:

$$\mathbf{D_m} = \frac{1}{1-\nu^2}\begin{bmatrix} E_1 & 0 & 0 \\ 0 & E_2 & 0 \\ 0 & 0 & \bar{G} \end{bmatrix} \text{ and } \bar{G} = \frac{E_1 + E_2}{4} \qquad \text{Equation 16}$$

Since the described masonry constitutive matrix is defined along the local principal axes of strains, this matrix needs to be transformed to the global coordinate system following the transformation relations:

$$\bar{\mathbf{D}}_\mathbf{m} = \mathbf{T}^T \mathbf{D_m} \mathbf{T} \qquad \text{Equation 17}$$

$$\mathbf{T} = \begin{bmatrix} \cos^2\theta & \sin^2\theta & \cos\theta\sin\theta \\ \sin^2\theta & \cos^2\theta & -\cos\theta\sin\theta \\ -2\cos\theta\sin\theta & 2\cos\theta\sin\theta & \cos^2\theta - \sin^2\theta \end{bmatrix} \qquad \text{Equation 18}$$

where θ is the inclination between the maximum principal axis and the global x-axis.. The constitutive matrix of steel which is normally aligned with the global x- and y-directions is defined as:

$$\mathbf{D_s} = \begin{bmatrix} \rho_{sh} E_{sx} & 0 & 0 \\ 0 & \rho_{sv} E_{sy} & 0 \\ 0 & 0 & 0 \end{bmatrix} \qquad \text{Equation 19}$$

where E_{sx} and E_{sy} are the secant moduli of steel in the x- and y-directions respectively. The global constitutive matrix is constructed by adding the two foregoing matrices:

$$\mathbf{D}_{global} = \bar{\mathbf{D}}_\mathbf{m} + \mathbf{D_s} \qquad \text{Equation 20}$$

FINITE ELEMENT PROGRAM AND SOLUTION ALGORITHM

The finite element program utilizes a plane stress, isoparametric, quadrilateral, eight-node element with the nonlinear constitutive relation and biaxial strength envelope as described in the previous sections. 3 x 3 Gauss points is used. The effect of steel bars is smeared over the masonry elements using an adjoining layer connected to the masonry element at each node (Figure 6). It assumes that steel and masonry have perfect contact. However, bond-slip between masonry and steel is included through the tension stiffening model of the masonry. While masonry and reinforcement are described separately, the overlaid elements are treated as one combined element in the FE program.

In order to predict both the pre- and post-cracking response, a solution strategy that is not sensitive to an overall negative stiffness expected to occur in the post peak region is required. Since the conventional or modified load control Newton-Raphson algorithm often fails to

converge in the vicinity of the peak point, the arc-length incremental scheme [11] has been adopted as the solution strategy. A convergence criterion based on the magnitude of nodal displacements is employed. To prevent numerical instabilities and achieve adequate accuracy in the program, the convergence tolerance was set to 0.001 which has been recommended by other researchers [3, 9]. A premature termination was enforced when slow convergence was observed during the iteration process.

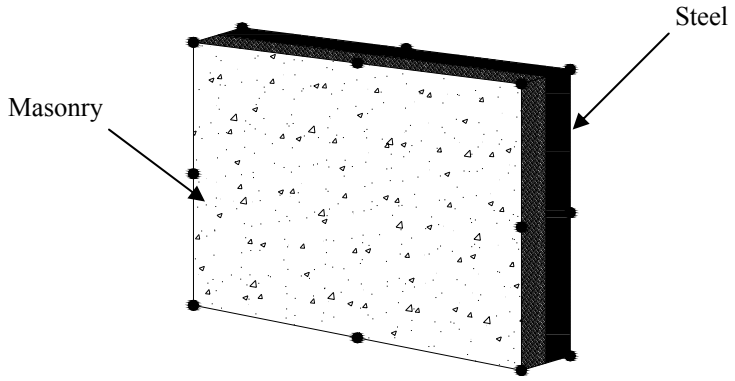

Figure 6 – Overlaid element of steel and concrete

EVALUATION TESTS

To evaluate the correlation of the analytical results with experimental data, six walls tested at University of Colorado as part of the TCCMAR research program [5] were selected. The walls were 1.8 m wide, 1.8 m high and 140 mm thick made of 6 inch concrete block units. Bond beam units were used throughout, which allowed the grout to completely fill the head joints. The vertical and horizontal reinforcement were relatively uniformly distributed in both directions and walls were fully grouted. The horizontal reinforcement was anchored to the extreme vertical reinforcement using 180-degree hooks. The walls were fabricated on a reinforced concrete base that was properly fixed to the floor. The loadings consisted of a constant vertical axial load and lateral shear load controlled by displacement increments. The reinforcement ratios and their properties including axial load for each wall are shown in Table 2.

Table 2 – Properties of the walls selected for evaluation test

Wall No.	Vertical Reinforcement				Horizontal Reinforcement				Axial Load (MPa)
	Qty.	ρ_s (%)	f_y (MPa)	f_u (MPa)	Qty.	ρ_s (%)	f_y (MPa)	f_u (MPa)	
6	5 15M	0.38	442	711	5 10M	0.14	400	587	0
4	5 20M	0.74	490	711	5 10M	0.14	400	587	0
12	5 15M	0.38	442	718	5 13M	0.24	462	738	0.69
5	5 20M	0.74	490	711	5 10M	0.14	400	587	0.69
2	5 15M	0.38	442	711	9 10M	0.24	386	566	1.86
3	5 20M	0.74	511	766	5 10M	0.14	386	566	1.86

The material properties used in the analysis were as follows: Uniaxial compressive strength $f'_m = 20.1$ MPa, Strain at peak strength $\varepsilon_o = 0.0026_{\text{mm/mm}}$, Tensile cracking strength $f_{cr} = 0.7$ MPa, Elastic modulus of masonry $E_m = 20{,}000$MPa, Poisson's ratio $\nu = 0.16$ and Reinforcement hardening parameter of $\zeta = 2\%$. Referring to Table 1, the tension stiffening parameter was chosen between 0.08 and 0.25 based on the steel ratio. Regarding the parameters describing constitutive relation and failure envelope, the following values were used in the analysis [5]:

$$A_o = 3.65,\ A_1 = 2.0,\ A_2 = 2.0,\ A_3 = 0.1,\ A_4 = 0.6 \qquad \text{Equation 21}$$

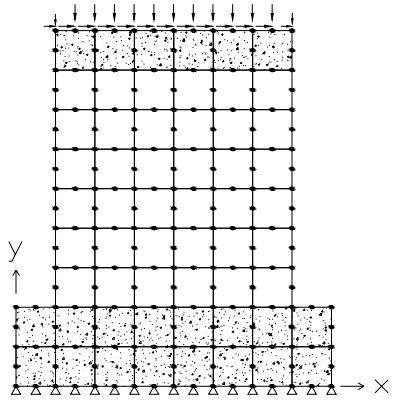

Figure 7 – Finite element model of the tested walls

As shown in Figure 7, the wall was modelled using 36 eight-node quadrilateral elements. The model included the concrete base and top beam simulated as relatively rigid members using elastic plane stress elements with much higher elastic modulus compared to the value used for masonry. The wall was restrained at the bottom in both the *x*- and *y*-directions. To simulate the boundary conditions of the top beam, all nodes at the top level were constrained to have equal displacement in the *x*-direction. The constant axial load was applied from the beginning of the analysis and an adaptive displacement controlled loading scheme (based on the arc-length algorithm) was employed as a solution strategy. A maximum of 30 iterations and a convergence threshold of 0.001 were selected in this regard.

Figure 8 shows the load-deflection curves for monotonically applied loading obtained from the FE analyses versus the cyclic response of Walls 6 and 3. Stable hysteresis loops and low degradation of stiffness in Wall 6 (Figure 8-a) correspond to a flexural failure which is closely predicted by the finite element analysis. On the other hand, presence of the axial load and increase of vertical steel changed the mode of deformation from a ductile flexural mode to a brittle shear mode in Wall 3 (Figure 8-b). Considering both halves of the hysteresis loops, the overall comparison indicates good agreement between experimental results and analytical predictions in terms of initial stiffness and ultimate strength especially for the flexural failure mode. As was expected, the results show some discrepancies due to the different load histories (monotonic versus cyclic). Cyclic loading gradually softens and degrades the masonry response. In monotonic loading, the integrity of the wall is not pre-damaged by reversing cycles and, therefore, higher strength and lower ductility are achieved. The overall results at the peak loads for all six tests are presented in Table 3 and Figure 9.

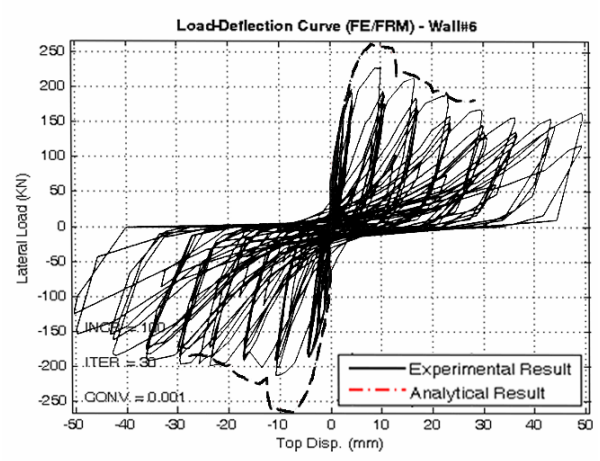

(a) Flexural failure mode (Wall 6)

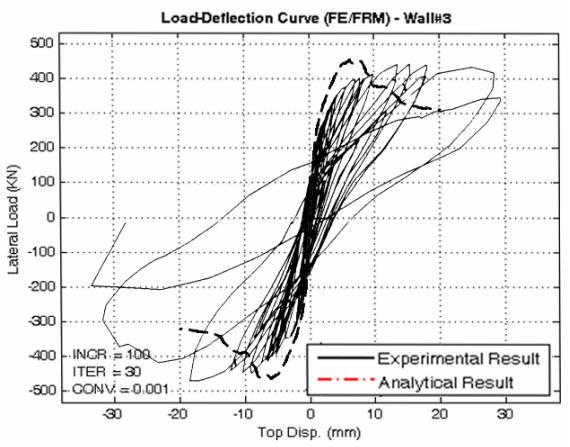

(b) Shear failure mode (Wall 3)

Figure 8 – Load-deflection path of analytical model and experiments

Table 3 – Comparison of experimental and analytical results in terms of peak load

Wall No.	Test Results		Analysis Result (KN)	Failure Mode
	Positive Peak Load (KN)	Negative Peak Load (KN)		
6	231	214	262	F
4	320	387	390	F
12	316	316	311	F
5	396	374	412	F
2	369	436	385	SH
3	445	467	463	SH

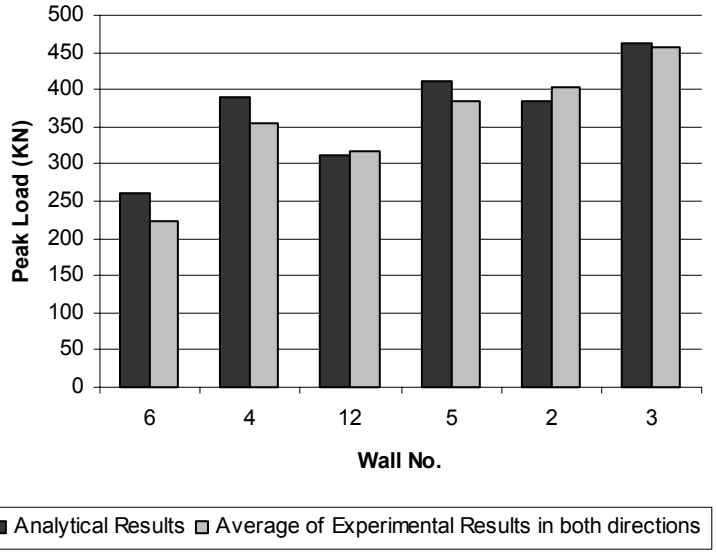

Figure 9 – Analytical peak loads versus average experimental results

SUMMARY AND CONCLUSION

The objective of this study was to evaluate use of the smeared crack approach for the nonlinear FE analysis of reinforced masonry walls subject to in-plane shear and axial loads. A layered finite element model was utilized where masonry and reinforcement were modelled separately using plane stress overlaid hybrid elements. Masonry was represented by an orthotropic behaviour along principal strain directions at each Gauss point. Compressive strength increase due to lateral confinement and strength reduction caused by crack development were included in the masonry model. The bond-slip between steel and concrete was considered as a tension stiffening property of the masonry. The comparison between analytical and experimental results showed good accuracy in prediction of initial stiffness and ultimate strength for different failure modes. The pre- and post-peak predictions for flexural failures were more representative than for shear failure where post-peak response under monotonic loading predicted greater degradation of strength than observed under post-peak cyclic loading. Mortar joints were not treated as planes of weakness in this study owing to the continuous solid columns of grouts in both directions. However research on the effect of discontinuous or partially grouted conditions is required. Also, the current constitutive relations (from concrete) should be modified for masonry materials.

ACKNOWLEDGEMENTS

This research was carried out as part of the mandate of the McMaster University Centre for Effective Design of Structures funded through Ontario Research and Development Challenge Fund.

REFERENCES

1. Page, A. W., Finite Element Model for Masonry, Journal of Structural Div. ASCE, Vol. 104, No. ST8 Aug. 1978, pp.1267-1285
2. Zucchini, A., P. B. Lourenco, A micro-mechanical model for the homogenization of masonry, Int. J. Solids and Structures, 39(2002), pp. 3233-3255
3. Lotfi H. R., P. B. Shing, An Appraisal of Smeared Crack Models for masonry Shear Wall Analysis, Computers and Structures, Vol. 41, No. 3, pp. 413-425, 1991
4. Ali S., A. W. Page, Cracking Analysis of Solid Concrete Masonry Subjected to Concentrated Loads, ACI Structural Journal, Vol. 86, No. 4, pp. 367-375, 1989
5. Edwing, R. D., Ahmad M. El-Mustapha, J. C. Kariots, FEM/I – A Finite Element Computer Program for the non-linear Static Analysis of Reinforced Masonry Building Components, U.S. – Japan Coordinate program for masonry Building research, Report No. 2.2-1, 1987 (Revised 1990)
6. Criesfiled, M. A., J. Wills, Analysis of RC Panels Using Different Concrete Models, Journal of Engineering Mechanics, ASCE, Vol. 115, No. 3, pp. 578-597.
7. Kupfer HB, Hilsdorf HK, Rusch H., Behaviour of Concrete under Biaxial Stresses, ACI Journal, Vol. 66, No. 8, pp. 656-666, 1969.
8. Vecchio, F. J., M. P. Collins, The Modified Compression-Field Theory for Reinforced Concrete Elements Subjected to Shear, ACI Structural J., Vol. 83, No. 2, pp. 219-231, 1986.
9. Kwak, H. G., D.Y. Kim, Nonlinear Analysis of RC shear walls considering tension-stiffening effect, Journal of Computers and Structures, Vol. 79(2001), pp.499-517
10. Darwin, D., Pecknold DA. Nonlinear Biaxial Stress-Strain Law for Concrete, Journal of Engineering Mechanics, Vol. 103, pp. 229-241, 1977
11. Crisfield, M. Nonlinear Finite Element Analysis of Solids and Structures, John Wilely & Sons, Inc., New York, N.Y., 1997